Chinese Chemical Letters 35 (2024) 109117

Contents lists available at ScienceDirect

Chinese Chemical Letters

journal homepage: www.elsevier.com/locate/cclet

Electron-transporting boron-doped polycyclic aromatic hydrocarbons: Facile synthesis and heteroatom doping positions-modulated optoelectronic properties

Tingting Huang[a,b], Zhuanlong Ding[a,b], Hao Liu[a], Ping-An Chen[c], Longfeng Zhao[c], Yuanyuan Hu[c], Yifan Yao[a], Kun Yang[a,b,*], Zebing Zeng[a,b,*]

[a] Key Laboratory of Chemo/Biosensing and Chemometrics, College of Chemistry and Chemical Engineering, Hunan University, Changsha 410082, China
[b] Shenzhen Research Institute of Hunan University, Shenzhen 518000, China
[c] Key Laboratory for Micro/Nano Optoelectronic Devices of Ministry of Education and Hunan Provincial Key Laboratory of Low-Dimensional Structural Physics and Devices School of Physics and Electronics, Hunan University, Changsha 410082, China

ARTICLE INFO

Article history:
Received 4 July 2023
Revised 13 September 2023
Accepted 17 September 2023
Available online 22 September 2023

Keywords:
Polycyclic aromatic hydrocarbon
Optoelectronic properties
Heteroatom doping
n-Type organic semiconductors
Structure–property relationship

ABSTRACT

While heteroatom doping serves as a powerful strategy for devising novel polycyclic aromatic hydrocarbons (PAHs), the further fine-tuning of optoelectronic properties *via* the precisely altering of doping patterns remains a challenge. Herein, by changing the doping positions of heteroatoms in a diindenopyrene skeleton, we report two isomeric boron, sulfur-embedded PAHs, named *Anti*-B_2S_2 and *Syn*-B_2S_2, as electron transporting semiconductors. Detailed structure-property relationship studies revealed that the varied heteroatom positions not only change their physicochemical properties, but also largely affect their solid-state packing modes and Lewis base-triggered photophysical responses. With their low-lying frontier molecular orbital levels, n-type characteristics with electron mobilities up to 1.5×10^{-3} cm^2 V^{-1} s^{-1} were achieved in solution-processed organic field-effect transistors. Our work revealed the critical role of controlling heteroatom doping patterns for designing advanced PAHs.

Polycyclic aromatic hydrocarbons (PAHs) have attracted increasing attentions over the past decade due to their intriguing physiochemical properties and enormous potential for widespread applications in the fields of optoelectronic devices such as organic light-emitting diodes (OLEDs), organic photovoltaics (OPVs), and organic field-effect transistors (OFETs) [1–6]. Among the various rationales for designing new PAHs and modulating their properties, the incorporation of main group elements, *i.e.*, the so-called heteroatom doping, represents one of the most powerful approach due to its unique capability of simultaneously fine-tuning the electronic structures and intermolecular noncovalent interactions of materials [7–9]. Specifically, due to its vacant p_z orbitals, boron atom can act concurrently as π-electron acceptors and Lewis acid and thus has been widely adopted for constructing novel boron-containing PAHs with suppressed lowest unoccupied molecular orbitals (LUMOs) energy levels, tuned aromaticity/antiaromaticity, intensive fluorescent emission, and robust Lewis acidity [10,11]. Therefore, miscellaneous B-doped PAHs with different boron doping numbers and positions have been prepared *via* sophisticated synthetic methodologies, among which the seminal examples include Yamaguchi's structurally constrained B-heterotriangulene derivatives, Piers and Tovar's seven-membered borepin-based ladder polycycles, Wanger and Wang's B-doped linear-fused high-order oligoacenes, and so on [12–22]. However, despite these elegant demonstrations, presently the material library of B-doped PAHs is severely limited, especially when compared to those based on other heteroatoms such as sulfur and nitrogen, thus severely hampering their further practical applications [10,23–28].

Among the manifold properties of B-containing π-conjugated materials that stemming from boron doping, the inherent electron-accepting capability is particularly appealing as it can potentially yield highly sought-after n-type semiconductors that hold broad applications in various optoelectronic devices. For instance, the B, N co-doped π-functional materials, as exemplified by the boron–nitrogen coordination bond-based conjugated polymers, have been widely applied in n-type OFETs/organic thermoelectrics and OPVs [29,30]. However, for the small-molecular B-doped PAHs, currently the electron transporting properties and related applications of the majority of these materials have been largely overlooked, especially for tricoordinate boron-containing ones that usually pos-

* Corresponding authors.
E-mail addresses: yangk@hnu.edu.cn (K. Yang), zbzeng@hnu.edu.cn (Z. Zeng).

https://doi.org/10.1016/j.cclet.2023.109117
1001-8417/

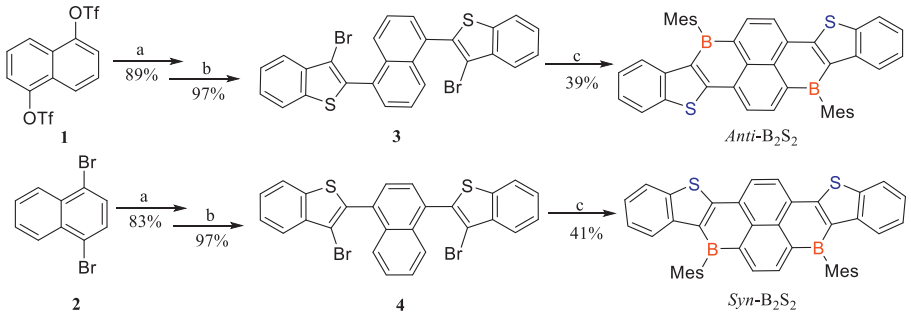

Scheme 1. Synthesis of *Anti*-B_2S_2 and *Syn*-B_2S_2, Reagents and conditions: (a) 2-Benzothienylboronic acid, $Pd(PPh_3)_4$, K_2CO_3 (2 mol/L in H_2O), dioxane, 90 °C, 12 h; (b) Br_2, DCM, r.t., 0.5 h; (c) i) *n*-BuLi (2.5 mol/L in hexane), toluene, 0 °C, 0.5 h; ii) BBr_3 (1 mol/L in hexane), 0 °C - reflux, toluene, overnight; iii) MesMgBr (1 mol/L in THF), toluene, r.t., 1 h.

sessing highly planar backbone configurations [31,32]. In addition, compared to the extensively explored B, N-doped PAHs [33–35], the investigations on the PAHs upon co-doping of boron and other atoms such as oxygen and sulfur have also been considerably neglected, thus leading to the influences of such co-doping on the physiochemical and charge transporting properties of the corresponding materials remains elusive [36,37].

In this context, herein, we presented the facile synthesis and systematic characterizations of two electron transporting B_2S_2-embedded diindenopyrenes molecules, namely *Anti*-B_2S_2 and *Syn*-B_2S_2, which feature isomeric boron/sulfur embedding positions. The investigation of their structure-property relationship revealed that the heteroatom orientations not only bring significantly changes on their various physicochemical properties such as optical absorption/emission and fluoride-activated photophysical responses, but also largely affect their solid-state packing modes. In addition, benefitted from their lower-lying LUMO energy levels, both B_2S_2 derivatives were exploited in solution-processed OFETs, showing promising unipolar n-type charge carrier mobilities up to 1.5×10^{-3} cm^2 V^{-1} s^{-1}, which ranks top amongst the few n-type semiconductors based on strictly three-coordinate boron-doped PAHs [38]. Our work highlighted the importance of heteroatom orientation patterns on modulating the physicochemical and charge transport properties of novel PAHs.

Scheme 1 depicted the three-step synthetic routes to the target doubly B-doped PAH molecules *Anti*-B_2S_2 and *Syn*-B_2S_2. Starting from commercially available 1,5-naphthalenebis(trifluoro methanesulfonate) (**1**) and 1,4-dibromonaphthalene (**2**), the dibromo compounds **3** and **4** were synthesized *via* standard palladium-catalyzed Suzuki coupling reaction and a sequential bromination step in good yields of 86% and 81%, respectively. Notably, due to their lack of solubilizing side chains, both **3** and **4** can be obtained upon direct precipitation from ethyl acetate with high purities instead of by tedious column chromatography procedures, which obviously should be beneficial for the facile and large-scale preparation of our final targeted PAHs. Both **3** and **4** were then subjected to a one-pot double-fold lithiation/trans-metalation and intramolecular electrophilic C–H borylation reactions upon treatment with mesityl magnesium bromide to afford *Anti*-B_2S_2 and *Syn*-B_2S_2 in overall yields of 39% and 41%, respectively, accompanying with excellent materials stability against air, water, and silica gels which allows them to be handled without special precautions. The two B-doped PAHs were fully characterized with NMR, HR-MS, and single crystallographic studies (*vide infra*), except for the ^{13}C NMR characterization of *Anti*-B_2S_2 due to its extremely poor solubility in common deuterated organic solvents. The ^{11}B NMR spectra of both compounds showed broad peaks at around 32-35 ppm, confirming the presence of three-coordinated boron atoms in their molecular architectures.

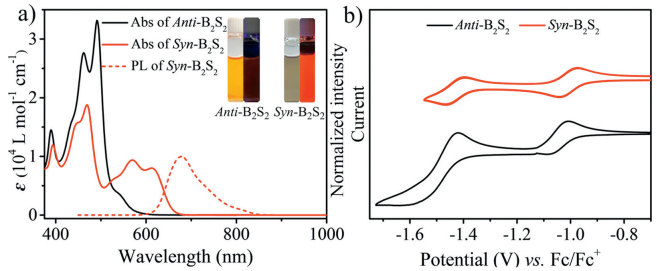

Fig. 1. (a) UV–vis absorption of *Anti*-B_2S_2 in toluene (10^{-4} mol/L), UV–vis absorption and normalized emission spectra of *Syn*-B_2S_2 in toluene (10^{-4} mol/L). Photo insets illustrate the sample under ambient light and 365 nm irradiation. (b) Cyclic voltammogram of *Anti*-B_2S_2 and *Syn*-B_2S_2 with 0.1 mol/L TBA-PF_6 as supporting electrolyte, Ag/AgCl as reference electrode, glassy carbon electrode as working electrode, Pt wire as the counter electrode.

The optical properties of the as-prepared *Anti*-B_2S_2 and *Syn*-B_2S_2 were first characterized by UV–vis spectroscopy. As illustrated in Fig. 1a, both compounds showed typically vibronic split bands in dilute solutions ascribing to their highly rigid conjugated backbone structures [39,40]. *Anti*-B_2S_2 exhibited a yellow color in solution featuring a maximum absorption wavelength (λ_{max}) of 492 nm with a shoulder at 462 nm, which can be assigned to HOMO-1→LUMO and HOMO-2→LUMO transitions, respectively, as suggested by time-dependent density-functional theory (TD-DFT) calculations (Fig. S1 and Table S1 in Supporting information). In contrast, *Syn*-B_2S_2 exhibited a wide absorption band with a red-shifted low energy absorption band peaking at 616 nm together with a $\lambda_{Abs}{}^{max}$ of 492 nm in solution state, corresponding to the HOMO→LUMO and HOMO-3→LUMO transitions, respectively (Fig. S2 and Table S2 in Supporting information). Interestingly, it was also found that while a fluorescent emission band approaching the NIR region featuring a maximum at 680 nm was found for *Syn*-B_2S_2 in its toluene solution with a fluorescence quantum yield (Φ_F) of 8.0% and lifetime (τ) of 4.0 ns, no such fluorescence was found for that of *Anti*-B_2S_2. This fluorescence quenching of *Anti*-B_2S_2 can be plausibly explained by the argument that its $S_0 \rightarrow S_1$ transition is symmetry forbidden as evidenced by the fact that the TD-DFT calculated oscillator strength (*f*) of the HOMO→LUMO transitions being 0 (Tables S1 and S2) [41,42]. In contrary, the $S_0 \rightarrow S_1$ transition of *syn*-isomer was symmetry allowed as suggested by its modest TD-DFT-calculated oscillator strength of 0.1665, which thus explained well for the observed fluorescence emission in the corresponding solution. Clearly, these results have revealed the substantial modulation effect of heteroatom doping patterns on the optical properties of the two B-doped PAH materials.

Table 1
Summary of the photophysical properties of *Anti*-B_2S_2 and *Syn*-B_2S_2.

Comps.	λ_{Abs} (nm)	E_g^{opt} (eV) [a]	E_{onset}^{red1} (V) [b]	E_{onset}^{red2} (V) [b]	$E_{1/2}^{red1}$ (V) [c]	$E_{1/2}^{red2}$ (V) [c]	HOMO [d] (eV)	LUMO [e] (eV)
Anti-B_2S_2	390, 462, 492	2.09	−0.99	−1.41	−1.00	−1.48	−5.90	−3.81
Syn-B_2S_2	315, 356, 394, 468, 570, 616	1.84	−0.93	−1.38	−1.01	−1.45	−5.71	−3.87

[a] Calculated from the onset of UV absorption.
[b] Onset potentials and [c] half-wave potentials, determined by cyclic voltammetric measurements and differential pulse voltametric measurements in 0.1 mol/L solution of TBA-PF_6 in CH_2Cl_2 *vs.* Fc/Fc^+, respectively.
[d] Calculated from $E_{HOMO} = E_{LUMO} - E_g^{opt}$.
[e] Estimated *vs.* vacuum level from $E_{LUMO} = -4.80\ eV - E_{onset}^{red1}$.

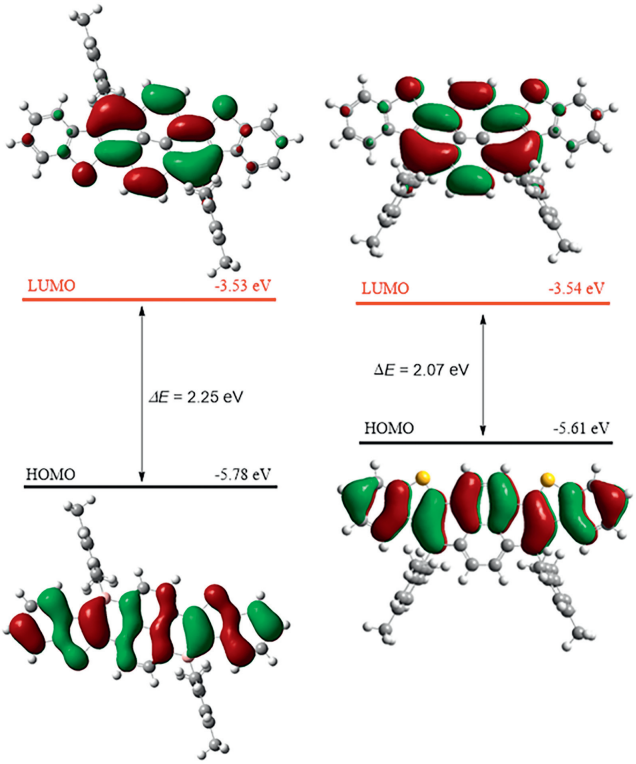

Fig. 2. Frontier molecular orbitals of *Anti*-B_2S_2 and *Syn*-B_2S_2 from DFT calculations at B3LYP/6-31G(d,p) level.

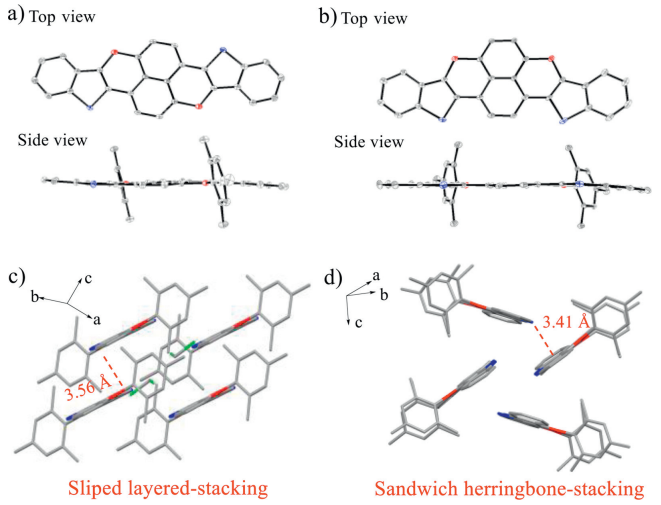

Fig. 3. Single-crystal structures and packing of *Anti*-B_2S_2 (a, c) and *Syn*-B_2S_2 (b, d). Mes group and hydrogen atoms were omitted for clarity in top view, the blue-, red- and green-colored atoms represent S, B and Cl atoms.

Cyclic voltammetry (CV) measurements were then carried out to investigate the electrochemical properties of *Anti*- and *Syn*-B_2S_2 in dichloromethane solutions at room temperature. As shown in Fig. 1b, two reversible reduction waves were found for both PAHs with onset potentials of the first/second reduction of −0.99/−1.41 V and −0.93/−1.38 V *vs.* Fc/Fc^+ for *Anti*-B_2S_2 and *Syn*-B_2S_2, respectively. These values, to the best of our knowledge, are amongst the mildest reduction potentials reported for boron-doped PAHs [7,10,43], thus reflecting the high electron deficiency of both molecules. Indeed, based on their first reduction onset potentials, substantial deep-lying LUMO energy levels of < −3.8 eV were obtained for both molecules (*Anti*-B_2S_2: −3.81 eV, *Syn*-B_2S_2: −3.87 eV), which can be ascribed to the presence of two strong electron-accepting tricoordinate boron atoms. Meanwhile, despite the doping of S atoms has been widely reported for enabling p-type characteristics with low ionization energy [44], no discernible oxidization waves were observed for both PAHs up to an electrochemical voltage of 2.0 V, which correlated well with the low-lying HOMO levels of two doped PAHs (*Anti*-B_2S_2: −5.90 eV, *Syn*-B_2S_2: −5.71 eV) as calculated on the basis of their optical bandgaps and LUMO energy levels (Table 1). Therefore, the simultaneously low-lying LUMO and HOMO levels of *Anti*-B_2S_2 and *Syn*-B_2S_2 might imply the potential of those two PAHs as unipolar n-type (electron-transporting) materials in optoelectronic devices.

To gain insight of the electronic structures and frontier molecular orbitals (FMOs) of two compounds, DFT calculations were further performed using the Gauss 09 program at the B3LYP/6-31G (d,p) level. As depicted in Fig. 2, *Anti*-B_2S_2 and *Syn*-B_2S_2 exhibited similar distributions of LUMOs, which were mainly located at the pyrenes, sulfur atoms and boron atoms of the conjugated skeletons, thus resulting in quite similar LUMO energy levels of −3.53 eV and −3.54 eV for *Anti*-B_2S_2 and *Syn*-B_2S_2, respectively, both of which were significantly lower than those of their non-doped parent diindenopyrenes by ~0.7 eV [45]. However, for the HOMOs, while that of *Anti*-B_2S_2 exhibited a nearly full delocalization of orbitals over its π-conjugated backbone, a shrink distribution of HOMOs was found for *Syn*-B_2S_2, showing that no orbital electron clouds were delocalized onto the two sulfur atoms and one of the benzene rings in its central naphthalene core. Accordingly, substantial discrepant HOMO energy levels of −5.78 and −5.61 eV were observed for *Anti*-B_2S_2 and *Syn*-B_2S_2, respectively, which again, were significantly lower than those of their non-doped parent diindenopyrenes by ~0.9 eV [45]. The lower HOMO energy level of *Anti*-B_2S_2 against that of *Syn*-B_2S_2 might be attributed to the engagement of electron-deficient boron atoms in the corresponding HOMO orbitals. Therefore, the calculated band gap of two molecules were 2.25 and 2.07 eV for *Anti*-B_2S_2 and *Syn*-B_2S_2, respectively, agreeing well with the trend as observed for those extracted from their optical absorption spectra. To evaluate the effect of boron-doping on their electronic structures, nucleus-independent chemical shifts (NICS) values and the anisotropy of the induced current density (ACID) plots were also calculated, showing that all the boron-containing hexacycles for both doped

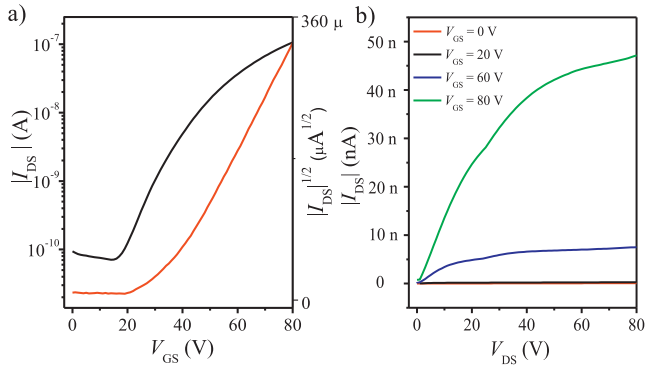

Fig. 4. Transfer (a) and output (b) characteristics of *Syn*-B_2S_2 based bottom-gate top-contact OFETs (I_{DS} = source-drain current, V_{GS} = gate voltage, V_{DS} = source-drain voltage channel length/width: 40/1000 (μm).

PAHs have positive NICS(1)$_{zz}$ values (~+16.9 ppm) and counter-clockwise ring current (Fig. S5 in Supporting information), which thus revealed that the introduction of the boron atom have rendered antiaromaticity to the corresponding hexacycles of the PAHs.

Single crystals of *Anti*-B_2S_2 and *Syn*-B_2S_2 that suitable for X-ray crystallography studies were successfully obtained by diffusing of *n*-hexane into their dichloromethane solutions at −20 °C. Both B-doped compounds exhibited highly planar conjugated backbones with their triaryl boron atoms retaining trigonal planar geometry and sums of bond angles around boron atoms approaching 360° (Figs. 3a and b). For the packing structures, however, due to the presence of two bulky pedant mesityl groups which were found to be aligned perpendicularly to the π-conjugated backbones, relatively less ordered but significantly distinct stacking modes were observed for two PAH molecules in crystalline states. For instance, *Anti*-B_2S_2 molecules adopt a layered-stacking structure to form slipped π stacks along the *c*-axis with an inter-layer distance of 3.56 Å, accompanied by two cocrystallized dichloromethane molecules contacting with the π-skeletons *via* hydrogen bonding interactions (Figs. 3c and Fig. S6 in Supporting information). In contrast, the syn isomer *Syn*-B_2S_2 exhibited a sandwich herringbone stacking mode to form a tetramer-like assemblies-based 3D superstructures [46], which is mainly driven by C–C contacts between the peripheral phenyl rings and the benzothiophene rings as well as S–C contacts between the *Syn*-B_2S_2 core and the benzothiophene rings (Fig. 3d and Fig. S7 in Supporting information). Clearly, these results indicate that the embedding orientations of boron and sulfur atoms in the π-scaffolds have significantly influenced the molecular packing modes of the corresponding PAHs molecules in the solid-state.

Given the low HOMO/LUMO energy levels of *Anti*-B_2S_2 and *Syn*-B_2S_2, we envisioned that both B-doped molecules might serve as a class of unipolar electron-transporting semiconductors. Therefore, to evaluate their charge transport properties, solution-processed thin film-based organic field-effect transistors (OFETs) were then fabricated with a Glass/Cr/Cu/OSC/Cytop/Al configuration based on the two doped PAHs. As shown in Fig. 4 and Fig. S8 (Supporting information), while the *Anti*-B_2S_2-based devices exhibited a relatively poor electron mobility (μ_e) of 3.5 × 10^{-5} cm^2 V^{-1} s^{-1}, a ~40-fold increased μ_e of 1.5 × 10^{-3} cm^2 V^{-1} s^{-1} was found for devices of *Syn*-B_2S_2, thus suggesting the higher efficiency of charge transport for the syn isomer in the thin-film states, which might be associated with its relatively higher film crystallinity as seen from their X-ray diffraction (XRD) patterns (Fig. S9a in Supporting information). Note, despite these values are only modest and the tetracoordinated boron-based molecules can give much higher mobilities [47,48], these values have ranked at the favorable positions among the μ_es results for the few tricoordinate boron-containing PAHs as reported as n-type semiconductors in OFETs [38,49–51], especially when considering the relatively amorphous nature of both compounds in thin-film states as evidenced by their atomic force microscopy (AFM) images (Fig. S9b in Supporting information) and XRD results.

It is well known that the tricoordinate boron-containing π-conjugated systems could act as Lewis acids to accommodate electron lone pairs from Lewis bases, thus resulting in significant variations of physiochemical property which can render them potentials in applications such as chemosensor. Therefore, as a class of typical triarylboron derivatives, a Lewis acid-base titration experiment with fluorine ions was carried out for both *Anti*-B_2S_2 and *Syn*-B_2S_2 in order to investigate their Lewis acidic characteristics. As shown in Fig. 5a, upon treatment with tetrabutylammonium fluoride (TBAF) solution, both B, S-embedded PAHs exhibited both significantly changes that can be readily observed both spectroscopically and with naked eyes. For instance, for *Anti*-B_2S_2, while its long-wavelength absorption band at 480 nm was gradually diminished, new absorption peaks were simultaneously emerged in the short wavelength region of 350–450 nm, thus resulting in an obvious solution color change from yellow to light green after the addition of TBAF, which should be attributed to the alterations of molecular electronic structures upon the binding of boron atoms with fluoride ions. Interestingly, unlike most of organoboron compounds that showing quenching of fluorescence after the fluoride treatment [29,39,52], a fluorescence turn-on phenomenon was found for the *anti*-isomer upon fluoride titration, thus implying

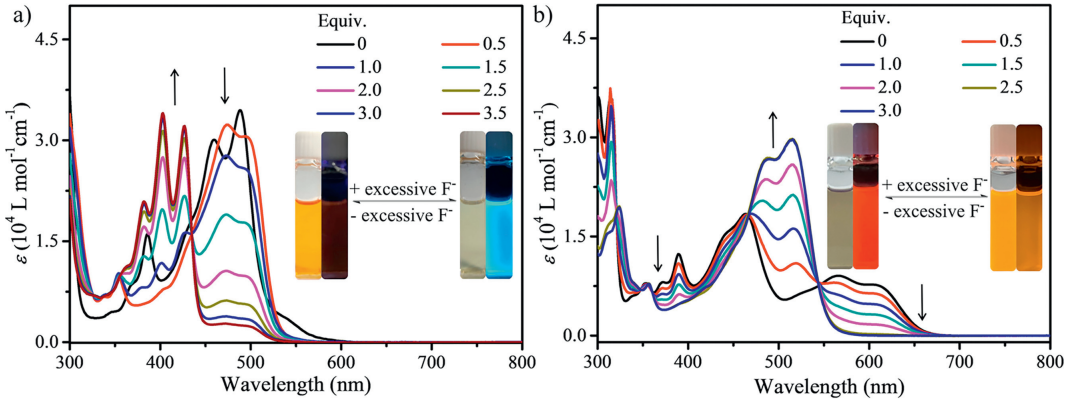

Fig. 5. UV–vis spectra of (a) *Anti*-B_2S_2 (1×10^{-4} mol/L in toluene) and (b) *Syn*-B_2S_2 (1.0×10^{-4} mol/L in toluene) upon the addition of TBAF. Photo insets illustrate sample appearance before and after addition of fluoride under ambient light and 365 nm irradiation.

the good potential of this materials as fluoride-activated fluorescent sensors. For *Syn*-B_2S_2, while significant colour change of from brown to orangish yellow was observed upon the adding of excessive TBAF, blue-shifted absorptions with similar peak diminishing and appearing phenomena were also generated together with two isosbestic points at 548 and 467 nm (Fig. 5b), thus implying that a possible transformation between this molecule with one single fluoride-bound product upon fluoride treatment [53]. Like the absorption, blue-shifted fluorescence from red to brownish yellow was further observed for *Syn*-B_2S_2, which represents a typical phenomenon of conjugated boron derivatives upon fluoride treatment. Thus, these results have clearly revealed the great capability of the changing of heteroatom doping positions for modulating the physicochemical properties of the resulting π-electron systems upon Lewis base treatments.

In summary, we have successfully synthesized two isomeric doubly B-doped PAHs with varied boron and sulfur orientation patterns *via* a facile synthetic approach. Through changing the orientations of boron/sulfur heteroatoms in their π-skeletons, the two PAHs exhibited distinct absorption/emission properties, modulated FMO energy levels, and significantly different intermolecular packing structures in crystalline states, and discrepant Lewis-base triggered photophysical responses. Most importantly, benefitting from their LUMO energy levels that arising from the doping of boron atoms, unipolar n-type semiconductors characteristics were observed for both PAHs in solution-processed OFETs with a highest electron mobility up to 1.5×10^{-3} cm^2 V^{-1} s^{-1}. For the few n-type semiconductors based on strictly three-coordinate boron-doped PAHs, *Syn*-B_2S_2 has relatively high electron mobility values in thin film state. This work shed some insights into how heteroatoms orientations of (hetero)PAHs affect their photophysical, electrochemical, and molecular stacking properties. Given the currently limited structural diversity of boron/sulfur-PAHs and the insufficient synthetic endeavours toward novel skeletons, the current work might open a new avenue to promote further development of boron/sulfur-embedded conjugated materials for optoelectronic applications.

Declaration of competing interest

The authors declare that they have no known competing financial interests or personal relationships that could have appeared to influence the work reported in this paper.

Acknowledgments

The authors thank the National Natural Science Foundation of China (Nos. 22375059, 22005133, 51922039 and 52273174), Shenzhen Science and Technology Program (No. RCJC20200714114434015), and Science and Technology Innovation Program of Hunan Province (No. 2020RC5033), and National Key Research and Development Program of China (No. 2020YFC1807302) for financial support.

Supplementary materials

Supplementary material associated with this article can be found, in the online version, at doi:10.1016/j.cclet.2023.109117.

References

[1] J.E. Anthony, Chem. Rev. 106 (2006) 5028–5048.
[2] A. Narita, X.Y. Wang, X. Feng, et al., Chem. Soc. Rev. 44 (2015) 6616–6643.
[3] Y. Sun, S. Gao, F. Lei, et al., Acc. Chem. Res. 48 (2015) 3–12.
[4] J. Chen, K. Yang, X. Zhou, et al., Chem. Asian. J. 13 (2018) 2587–2600.
[5] N. Liang, D. Meng, Z. Wang, Acc. Chem. Res. 54 (2021) 961–975.
[6] Y. Gu, Z. Qiu, K. Müllen, J. Am. Chem. Soc. 144 (2022) 11499–11524.
[7] M. Hirai, N. Tanaka, M. Sakai, et al., Chem. Rev. 119 (2019) 8291–8331.
[8] X. Wang, X. Yao, A. Narita, et al., Acc. Chem. Res. 52 (2019) 2491–2505.
[9] A. Borissov, Y. Maurya, L. Moshniaha, et al., Chem. Rev. 122 (2022) 565–788.
[10] E.V. Grotthuss, A. John, T. Kaese, et al., Asian J. Org. Chem. 7 (2018) 37–53.
[11] S.K. Mellerup, S. Wang, Trends. Chem. 1 (2019) 77–89.
[12] S. Saito, K. Matsuo, S. Yamaguchi, J. Am. Chem. Soc. 134 (2012) 9130–9133.
[13] L.G. Mercier, W.E. Piers, M. Parvez, Angew. Chem. Int. Ed. 48 (2009) 6108–6111.
[14] D.R. Levine, M.A. Siegler, J.D. Tovar, J. Am. Chem. Soc. 136 (2014) 7132–7139.
[15] S. Kirschner, J. Mewes, M. Bolte, et al., Chem. Eur. J. 23 (2017) 5104–5116.
[16] H. Wei, Y. Liu, T.Y. Gopalakrishna, et al., J. Am. Chem. Soc. 139 (2017) 15760–15767.
[17] L. Li, Y. Gao, C. Dou, et al., Chin. Chem. Lett. 31 (2020) 1193–1196.
[18] G. Liao, X. Chen, Y. Qiao, Org. Lett. 23 (2021) 5836–5841.
[19] P. Zhang, J. Zeng, F. Zhuang, et al., Angew. Chem. Int. Ed. 60 (2021) 23313–23319.
[20] J. Guo, K. Zhang, Y. Wang, et al., Chem. Sci. 14 (2023) 4158–4165.
[21] J. Guo, Z. Li, X. Tian, et al., Angew. Chem. Int. Ed. 62 (2023) e202217470.
[22] Y. Liu, L. Yuan, J. Guo, et al., Angew. Chem. Int. Ed. 62 (2023) e202306911.
[23] B. Li, W. Peng, S. Luo, et al., Org. Lett. 21 (2019) 1417–1421.
[24] Y. Wang, S. Qiu, S. Xie, et al., J. Am. Chem. Soc. 141 (2019) 2169–2176.
[25] F. Kang, J. Yanga, Q. Zhang, J. Mater. Chem. C 10 (2022) 2475–2493.
[26] T. Luo, Y. Wang, J. Hao, et al., Angew. Chem. Int. Ed. 62 (2023) e202214653.
[27] Z. Li, Y. Tang, J. Guo, et al., Chem 9 (2023) 1281–1294.
[28] K. Zhang, J. Guo, H. Liu, et al., Chem. Commun. 59 (2023) 4947–4950.
[29] R. Zhao, J. Liu, L. Wang, Acc. Chem. Res. 53 (2020) 1557–1567.
[30] J. Miao, Y. Wang, J. Liu, et al., Chem. Soc. Rev. 51 (2022) 153–187.
[31] Sun Z, S. Li, Z. Liu, Chin. Chem. Lett. 27 (2016) 1131–1138.
[32] S.K. Mellerupab, S. Wang, Chem. Soc. Rev. 48 (2019) 3537–3549.
[33] X. Wang, J. Wang, J. Pei, Chem. Eur. J. 21 (2015) 3528–3539.
[34] J. Wang, J. Pei, Chin. Chem. Lett. 27 (2016) 1139–1146.
[35] C.R. McConnell, S.Y. Liu, Chem. Soc. Rev. 48 (2019) 3436–3453.
[36] T. Jin, L. Kunze, S. Breimaier, et al., J. Am. Chem. Soc. 144 (2022) 13704–13716.
[37] Y. Chang, Y. Wu, X. Wang, et al., Chem. Eng. J. 451 (2023) 138545–138554.
[38] J.M. Farrell, C. Mützel, D. Bialas, et al., J. Am. Chem. Soc. 141 (2019) 9096–9104.
[39] J. Zhang, F. Liu, Z. Sun, et al., Chem. Commun. 54 (2018) 8178–8181.
[40] K. Yang, X. Zhang, A. Harbuzaru, et al., J. Am. Chem. Soc. 142 (2020) 4329–4340.
[41] H. Kubo, T. Hirose, K. Matsuda, Org. Lett. 19 (2017) 1776–1779.
[42] Yi. Wu, S. Ying, L. Su, et al., J. Am. Chem. Soc. 144 (2022) 10736–10742.
[43] C. Mützel, J.M. Farrell, K. Shoyama, et al., Angew. Chem. Int. Ed. 61 (2022) e202115746.
[44] T. Okamoto, C.P. Yu, C. Mitsui, et al., J. Am. Chem. Soc. 142 (2020) 9083–9096.
[45] D. Hibi, K. Kitabayashi, K. Fujita, et al., J. Org. Chem. 81 (2016) 3735–3743.
[46] S. Fratini, M. Nikolka, A. Salleo, et al., Nat. Mater. 19 (2020) 491–502.
[47] Y. Min, C. Dou, H. Tian, et al., Angew. Chem. Int. Ed. 57 (2018) 2000–2004.
[48] Y. Min, C. Dou, D. Liu, et al., J. Am. Chem. Soc. 141 (2019) 17015–17021.
[49] K. Matsuo, S. Saito, S. Yamaguchi, J. Am. Chem. Soc. 136 (2014) 12580–12583.
[50] K. Matsuo, S. Saito, S. Yamaguchi, Angew. Chem. Int. Ed. 55 (2016) 11984–11988.
[51] T. Kushida, S. Shirai, N. Ando, et al., J. Am. Chem. Soc. 139 (2017) 14336–14339.
[52] Z. Zhou, A. Wakamiya, T. Kushida, et al., J. Am. Chem. Soc. 134 (2012) 4529–4532.
[53] M. Lepeltier, O. Lukoyanova, A. Jacobson, et al., Chem. Commun. 46 (2010) 7007–7009.